Catal Lett (2008) 125:331–339
DOI 10.1007/s10562-008-9569-3

Oxidative Dehydrogenation of Ethane to Ethylene with Carbon dioxide over Cr–Ce/SBA-15 Catalysts

Xuejun Shi · Shengfu Ji · Kai Wang

Received: 11 June 2008 / Accepted: 28 June 2008 / Published online: 16 July 2008

Abstract Chromium oxide supported on SBA-15 was modified with Ce species by an incipient method. The effect of Ce on the activity of Cr/SBA-15 catalyst in the dehydrogenation of ethane with CO_2 was investigated. The activity is enhanced for Ce modified Cr/SBA-15 catalyst for the dehydrogenation of ethane with CO_2. The cycle between Cr^{6+} and Cr^{3+} species can be carried out viaing the dehydrogenation of ethane and oxidation of CO_2 processes.

Keywords Dehydrogenation · Chromium oxide · Heterogeneous catalysis · CO_2 · XPS

1 Introduction

The oxidative dehydrogenation (ODH) of ethane to ethylene by O_2 was an important process as an alternation to thermal cracking of ethane. However, the challenge of this reaction was to avoid over-oxidation in order to obtain high selectivity towards ethylene. In the last decade, the dehydrogenation of ethane by carbon dioxide has received much attention [1–6]. Carbon dioxide is a promising oxidant for dehydrogenation of ethane. In the dehydrogenation reaction, CO_2 is expected (1) to serve as a medium for supplying heat to the endothermic dehydrogenation reaction, (2) to increase equilibrium conversion by diluting light alkanes, and (3) to maintain the activity of the catalyst over a long time by removing coke formed on the catalyst.

X. Shi · S. Ji (✉) · K. Wang
State Key Laboratory of Chemical Resource Engineering, Beijing University of Chemical Technology, 15 Beisanhuan Dong Road, P.O. Box 35, Beijing 100029, China
e-mail: jisf_buct@live.cn

Nakagawa et al. [7] studied the dehydrogenation of ethane by carbon dioxide over several oxides and found that gallium oxide was an effective catalyst for this reaction, giving 18.6% ethylene yield with a selectivity of 94.5% at 650 °C. Takahara and Saito [8] reported the promoting effect of carbon dioxide on dehydrogenation of propane over supported Cr_2O_3 catalysts. They found that carbon dioxide exerted a promoting effect only on SiO_2-supported Cr_2O_3 catalysts.

Many research results [1, 3, 4] showed the supported Cr-based catalysts exhibited excellent performances for the ODH reaction. Mimura et al. [4] found that Cr/H-ZSM-5(with $SiO_2/Al_2O_3 > 1{,}900$) presented high performance in the ODH of ethane to ethylene with CO_2. Liu et al. [1] studied the ODH of ethane by CO_2 over Cr/MSU-x catalyst and obtained the 68.1% ethane conversion and 55.6% ethylene yield at 700 °C. Wang et al. [3] investigated the effect of support such as Al_2O_3, SiO_2, TiO_2 and ZrO_2 on the catalytic ODH of ethane to ethylene with CO_2 over several supported Cr_2O_3 catalysts, and found the 8 wt.% Cr_2O_3/SiO_2 catalyst had better catalytic performance, giving a 61% ethane conversion and 55.5% ethylene yield. However the distribution of Cr_2O_3 on the supports and the surface chromium species structure, which determined the activity of catalysts, were influenced by the nature of supports. In view of the fact that, the support plays a decisive role in determining the dispersion of the active phase and in certain occasions, salt support interaction enhances the catalytic activity of the active phase enormously [9].

Ceria used as a reducible oxide support, can enhance the catalytic activity via metal-support interaction and/or improved dispersion of the active metal component [10, 11]. An important property of ceria is the oxygen storage capacity (OSC), i.e. the ability to adsorb and

release oxygen under oxidizing and reducing conditions [12]. In addition, ceria is found to stabilize the catalyst against deactivation due to a higher thermal stability and/or better dispersion of the active metal. Although CeO_2-based supports are stable at high temperatures they suffer from the drawbacks of high cost and relatively low surface areas [13, 14]. Recently, mesoporous silica SBA-15 [15, 16], which has highly ordered hexagonal structure with high surface areas of 600–1,000 m^2/g, adjustable pore sizes of 4.6–30 nm and wall thickness of 3.1–6.4 nm, has attracted wide attention as a new material for catalysts and catalyst supports. SBA-15 has successfully been applied as a support for various catalytically active phases [17–19]. The influence of solvents on the formation of metal and its oxides nanoparticles in SBA-15 was also investigated [20]. However, there is little literature about the catalyst using SBA-15 as support for the ODH of ethane with CO_2. In the present work, a series of catalysts using Cr as activity species, based on SBA-15 as the support and CeO_2 as the promoter, were prepared by the impregnation method, and their catalytic activity for ODH of ethane with CO_2 were investigated. The main goal is to explore the CeO_2 effect on the activity behavior of the catalysts for the ODH of ethane with CO_2.

2 Experimental

2.1 Catalyst Preparation

SBA-15 was synthesized according the literature [15]. Briefly, a solution of triblock copolymer EG_{20}-PG_{70}-EG_{20} (4 g)/2 M HCl (120 g)/water (32.4 g) was stirred for 2 h at 40 °C. 8.5 g of TEOS was added afterwards and the mixture was stirred overnight at 40 °C. The solution was transferred into Teflon bottle and aged at 100 °C for 24 h. The filtered and washed solids were dried at ambient temperature for 24 h, followed by calcination in air at 550 °C for 6 h.

Cr/SBA-15 catalysts with different Cr contents were prepared by wet impregnation of appropriate amounts of chromium nitrate on SBA-15 support. The samples were denoted as xCrSBA-15, where x was the mass percent of Cr metal, and in the range of 2.5–10.0%. Cr–Ce/SBA-15 catalysts were prepared by co-impregnation of pure SBA-15 with a specific concentration aqueous solution of Ce and Cr nitrates. All the catalysts were dried at 100 °C for 24 h and then calcined at 600 °C for 6 h.

2.2 Catalyst Characterization

X-ray powder diffraction (XRD) patterns of the catalysts were obtained on a Bruck D8 diffractometer using Cu K_α radiation at follows: 40 kV, 30 mA, 2θ scanning from 0.5° to 5° for the low-angle XRD and 40 kV, 40 mA, 2θ scanning from 10° to 80° for wide-angle XRD. N_2 sorption isotherms were obtained at liquid nitrogen temperature with a Thermo Electron Corporation Sorptomatic 1990 instrument. The samples were pretreated at 200 °C for 5 h, and the specific surface area of the samples was determined using the Brunauer–Emmett–Teller (BET) method. The pore volume and pore size distribution were derived from the desorption profiles of the isotherms using the Barrett–Joyner–Halanda (BJH) method. X-ray Photoelectron Spectroscopy (XPS) experiments were carried out on an Escalab250 instrument (Thermo Electron Corporation) using Al K_α as the exciting radiation at constant pass energy of 50 eV. Binding energies were calibrated by using the carbon present as a contaminant (C1s = 285.0 eV). The surface atomic compositions of all samples were calculated from photoelectron peak areas for each element after correcting for instrument parameters. Temperature programmed reduction (TPR) experiments were performed using a Thermo Electron Corporation TPD/D/R/O 1100 series catalytic surfaces analyzer equipped with a TCD detector. Samples were preheated with 10% O_2/He mixture heating 20 °C/min up to 600 °C and hold for 120 min, then cooling in flowing N_2 down to room temperature, and thereafter reduced with 5% H_2/N_2 mixture heating 20 °C/min up to 900 °C. For the used catalyst, the TPR experiment was performed without being pretreated in the 10% O_2/He atmosphere. Water produced by the sample reduction was condensed in a cold trap before reaching the detectors. Only H_2 was detected in the outlet gas confirming the effectiveness of the cold trap.

2.3 Catalytic Reaction

The ODH reaction was carried out using a fixed bed flow-type quartz reactor (i.d., 6 mm; length, 300 mm) with 200 mg of the catalyst (40–60 mesh) at atmosphere pressure. Prior to the test, the catalysts were pretreated at 600 °C in a flow of oxygen (O_2, 5 mL/min) for 1 h, and then cooling in flowing argon down to room temperature. The reaction was started by introducing a mixture gas of C_2H_6 and CO_2 or Ar to the reactor with a gas hourly space velocity (GHSV) of the 3,600 $mL/g_{cat.}$ h. The mole ratio of $V_{CO_2 \text{ or } Ar}/V_{C_2H_6}$ is 3. The intrinsic activation energy of the catalysts for the ODH of ethane with CO_2 were conducted with significantly low conversions which were usually controlled to be significantly lower than those defined by thermodynamic equilibrium by adjusting gas hourly space velocity. Rate limitation by external and internal mass transfer under differential conditions proved to negligible by applying suitable experimental criteria. The outlet products were analyzed after the reaction for 30 min on a gas chromatograph (Beijing East & West Electronics

Institute, GC-4000A) using TCD. The conversion, selectivity and TOF were calculated as follows:

$$C_2H_6 \text{ conversion} = 1 - \frac{2 \times n_{C_2H_6}}{2 \times n_{C_2H_6} + 2 \times n_{C_2H_4} + n_{CH_4}}$$

$$CO_2 \text{ conversion} = 1 - \frac{n_{CO_2}}{(n_{CO_2} + n_{CO})}$$

$$C_2H_4 \text{ selectivity} = \frac{2 \times n_{C_2H_4}}{2 \times n_{C_2H_4} + n_{CH_4}}$$

$$\text{TOF}\,(\text{mol}\,\text{s}^{-1}\ \text{mol}\,\text{Cr-atom}^{-1}) = C_{\text{product}} \times F_{\text{total}}/M_{\text{Cr-atom}}$$

where C_{product} is the concentration of products in the outlet gas observed by GC analysis (%), F_{total} is the flow rate of feed gas (mol s^{-1}), and $M_{\text{Cr-atom}}$ is the amount of Cr atoms in the catalyst (mol).

3 Results and Discussion

3.1 XRD Results

The low-angle XRD patterns of the Cr/SBA-15 and Cr–Ce/SBA-15 catalysts are shown in Fig. 1. The SBA-15 support (Fig. 1a) shows three well-resolved diffraction peaks in the 2θ range 0.7–2°, corresponding to the diffraction of (100), (110) and (200) planes. These peaks are characteristic of the hexagonally ordered structure of SBA-15 [15, 16]. When Cr is loaded onto SBA-15, the d_{100} peak shifts to higher angle, and the d_{100}, d_{110} and d_{200} peaks attenuate in intensity. This is consistent with previous reports in the literature [21]. It is possible that partly dispersed Cr species are embedded into the channel of SBA-15. In this case, the d-spacing of the 100 plane is decreased resulting in the shift of the d_{100} peak to higher angle. The XRD patterns of 5Cr–Ce/SBA-15 catalysts are essentially identical to that of Cr/SBA-15 catalyst.

Figure 2 shows the wide-angle XRD patterns of Cr/SBA-15 and 5Cr–Ce/SBA-15 samples. Clearly, the SBA-15 support exhibits a broad peak at 15–30 °C which is characteristic of amorphous silica. From Fig. 2a–d, it can be seen that the diffraction peak at 2θ = 24.5°, 33.5°, 36.2°, 41.4°, 50.2°, 54.8°, 63.5° and 65.1°, corresponding to the diffractions of (012), (104), (110), (113), (024), (116), (214), and (300) of Cr_2O_3 are observed over the Cr/SBA-15 catalysts. With the Cr content increasing from 2.5 to 10%, the intensity of Cr_2O_3 diffraction peak increases gradually. At the same time the Cr_2O_3 diffraction peak becomes sharper which indicates the particle of bulk Cr_2O_3 becomes bigger.

The diffraction peaks of CeO_2 are observed at 2θ scale followed by 28.5°, 33.2°, 47.5° and 56.3° corresponding to the (111), (200), (220) and (311) planes, which are the characteristic of cubic, fluorite structure of CeO_2 [22] (Fig. 2e–h). In addition, the diffraction peak intensity of Cr species decreases obviously after the loading of Ce species. There almost have no Cr species characteristic diffraction peaks over the 5Cr–15Ce/SBA-15 catalyst. This result suggests that the addition of Ce species markedly enhances the dispersion of the chromium species in the 5Cr–Ce/SBA-15 catalysts.

3.2 Textural Properties of Catalysts

The N_2 adsorption–desorption isotherms of SBA-15, 5Cr/SBA-15 and 5Cr–Ce/SBA-15 samples with different Ce

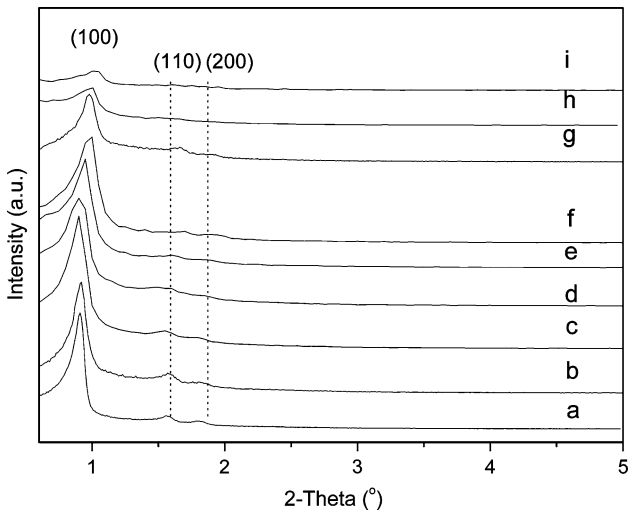

Fig. 1 Low-angle XRD patterns of the samples: (a) SBA-15; (b) 2.5Cr/SBA-15; (c) 5.0Cr/SBA-15; (d) 7.5Cr/SBA-15; (e) 10Cr/SBA-15; (f) 5Cr–5Ce/SBA-15; (g) 5Cr–7.5Ce/SBA-15; (h) 5Cr–10Ce/SBA-15; (i) 5Cr–15Ce/SBA-15

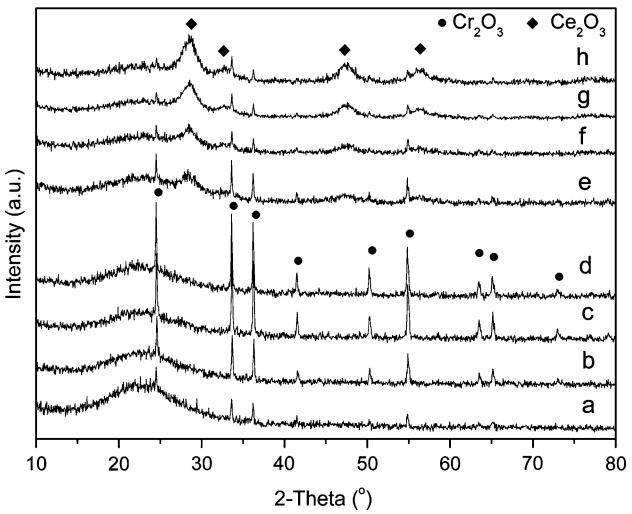

Fig. 2 Wide-angle XRD patterns of the samples: (a) 2.5Cr/SBA-15; (b) 5.0Cr/SBA-15; (c) 7.5Cr/SBA-15; (d) 10Cr/SBA-15; (e) 5Cr–5Ce/SBA-15; (f) 5Cr–7.5Ce/SBA-15; (g) 5Cr–10Ce/SBA-15; (h) 5Cr–15Ce/SBA-15

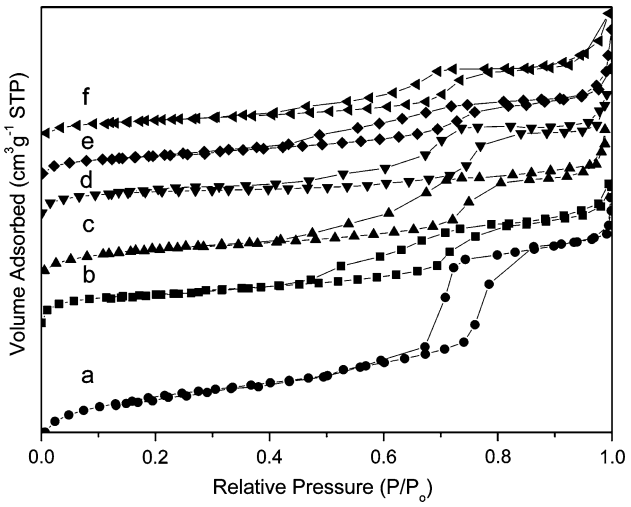

Fig. 3 N_2 adsorption–desorption isotherms of the samples: (a) SBA-15; (b) Cr/SBA-15; (c) 5.0Cr–5.0Ce/SBA-15; (d) 5.0Cr–7.5Ce/SBA-15; (e) 5.0Cr–10Ce/SBA-15; (f) 5.0Cr–15Ce/SBA-15

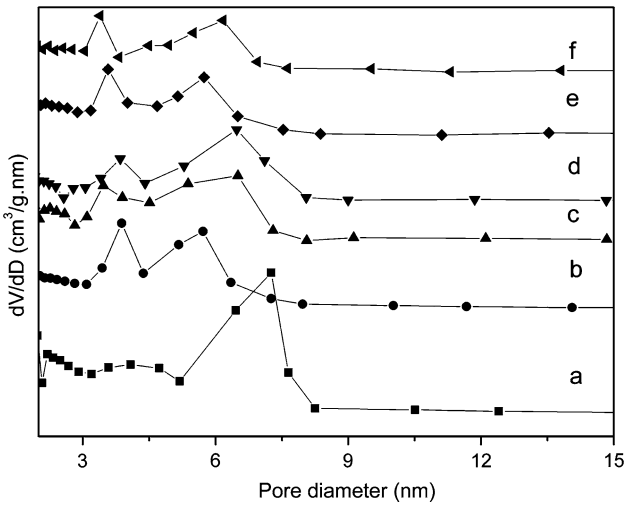

Fig. 4 Pore size distribution of the samples: (a) SBA-15 (b) 5Cr/SBA-15; (c) 5.0Cr–5.0Ce/SBA-15; (d) 5.0Cr–7.5Ce/SBA-15; (e) 5.0Cr–10Ce/SBA-15; (f) 5.0Cr–15Ce/SBA-15

content are shown in Fig. 3. The isotherms of SBA-15 support exhibits a typical IV features with H_1-type hysteresis loop, which is typical of mesoporous materials with one-dimensional cylindrical channels [15]. The sharp inflection between the relative pressure $P/P_0 = 0.6$–0.8 observed in the isotherm corresponds to capillary condensation within uniform mesopores and is also a function of the pore diameter. After the impregnation of Cr and Ce species, all the isotherms of the catalysts are similar with that of SBA-15 support. This suggests that the hexagonally ordered structure of SBA-15 remains in the samples. Whereas the hysteresis inflection is less sharp indicating that the pore size of the material is less ordered and uniform compared to that of the SBA-15 support. Simultaneity, the opening of the hysteresis loop at lower P/P_0 relative pressure is also observed with samples containing Cr and Ce species. This indicates that the pore size decreases on these samples. These results are in good agreement with those obtained by low-angle XRD results presented above.

The pore distributions of SBA-15, 5Cr/SBA-15 and the 5Cr–Ce/SBA-15 samples with different Ce content are shown in Fig. 4. The values of specific surface area (S_{BET}) and pore volume (V_p) show a monotonic decrease with the increase of cerium content (Table 1). For the SBA-15 support, the average pore size is 7.26 nm and the S_{BET} is 790.8 m^2/g. After the Cr and Ce species supported, the S_{BET} value decrease sharply. The decrease in the specific surface area of the SBA-15 after introducing of Cr and Ce species may be caused by the presence of extra-framework Cr and/or Ce species with lower surface area which can decrease the overall surface area of the final catalysts [23]. In addition, the anchoring of Cr and/or Ce species on the SBA-15 surface

Table 1 Textural and structural characteristics of the catalysts

Samples	S_{BET} (m^2/g)	V_p (cm^3/g)	D_{BJH} (nm)
SBA-15	790.80	1.13	7.26
5.0Cr/SBA-15	507.24	0.62	3.88, 5.72
5.0Cr–5.0Ce/SBA-15	439.71	0.58	3.47, 6.51
5.0Cr–7.5Ce/SBA-15	410.51	0.50	3.85, 6.48
5.0Cr–10Ce/SBA-15	373.15	0.48	3.57, 5.74
5.0Cr–15Ce/SBA-15	345.76	0.45	3.39, 6.17

also induces a decrease in the pore volume of the material indicating a partial blocking of the mesochannels during they introduction. It is thought that during the anchoring of Cr and/or Ce on the SBA-15 surface, some pore wall collapse should have occurred leading to the decrease of the pore size diameter. Similar result has been reported on the Al-SBA-15 system with high Al content [24].

As for all the catalyst samples, there are two types of pores with diameters of ca. 3.5 and 6.1 nm presented in the catalyst (Fig. 4). The former type of pores is attributed to the insertion of the Cr and/or Ce component into the pores of SBA-15 and subsequent partly blocks the channels of the SBA-15 material. The latter type of pores is the banana-like of SBA-15 with ordered pores [16].

3.3 XPS Results

Figure 5 illustrates the $Cr2p_{3/2}$ spectra of the 5Cr/SBA-15 and 5Cr–Ce/SBA-15 with different Ce content catalysts. And the surface concentrations of Cr species are given in Table 2. It has been reported that Cr ions exist in various oxidation states in supported chromium materials, in which

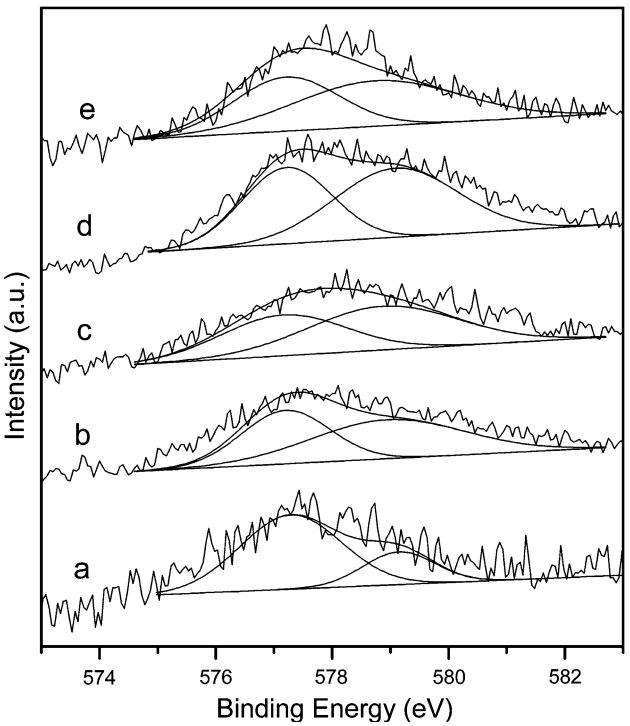

Fig. 5 XPS spectra of Cr_{2p} over the catalysts: (a) 5Cr/SBA-15; (b) 5.0Cr–5.0Ce/SBA-15; (c) 5.0Cr–7.5Ce/SBA-15; (d) 5.0Cr–10Ce/SBA-15; (e) 5.0Cr–15Ce/SBA-15

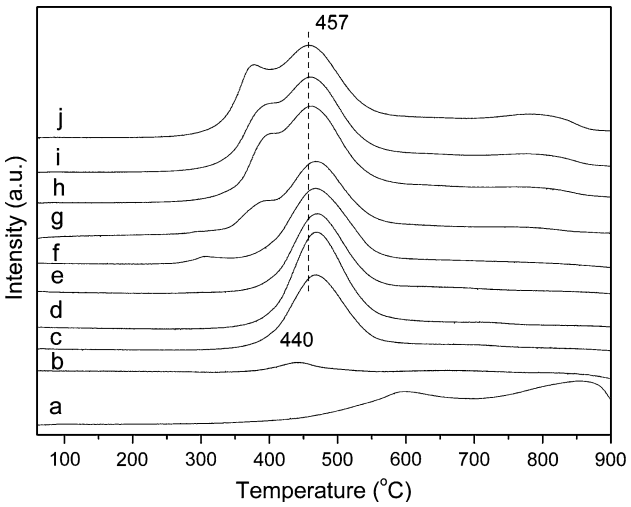

Fig. 6 TPR profiles of catalyst samples: (a) 10Ce/SBA-15; (b) bulk Cr_2O_3; (c) 2.5Cr/SBA-15; (d) 5.0Cr/SBA-15; (e) 7.5Cr/SBA-15; (f) 10Cr/SBA-15; (g) 5Cr–5Ce/SBA-15; (h) 5Cr–7.5Ce/SBA-15; (i) 5Cr–10Ce/SBA-15; (j) 5Cr–15Ce/SBA-15

Cr^{6+} and Cr^{3+} are believed to participate in redox processes in the catalytic oxidative dehydrogenation of alkanes [25–27]. An investigation on the oxidation states of Cr ions in/on catalysts is beneficial for the elucidation of the nature of the active sites. According to what have been reported in the literature [26–29], the Binding Energy (BE) of $Cr2p_{3/2}$ signals at ca. 577 eV could be assigned to Cr^{3+} ions whereas those at ca. 579 eV to Cr^{6+} ions. In this study, the curve fitting for the $Cr2p_{3/2}$ line show the presence of Cr^{3+} (ca. 577.2 eV) and Cr^{6+} (ca. 579.1 eV) in the catalysts (Fig. 5). The overall amount of chromium detected and the Cr^{6+}/Cr^{3+} ratio at the catalyst surface increases gradually with higher Ce loading from 0 to 10% (Table 2). Many researchers have investigated the dehydrogenation of light alkane over support Cr-based catalysts. The chromium species with the high oxidation state were the key to higher catalytic activity during the dehydrogenation of light alkane [30, 31]. Ge et al. [32] had used ESR and UV-DRS to probe the active site for the ODH of ethane with CO_2 over silica-supported chromium oxide catalyst, and found that species with high oxidation state (Cr^{5+} or Cr^{6+}) are important for the reaction. In this investigation, it is found that two Cr species, Cr^{3+} and Cr^{6+}, coexisted on the surface of the catalyst. The Cr^{6+}/Cr^{3+} ratios increases with Ce loading and reach the maximum (1.30) at 10% Ce loading. Whereas further increasing Ce content to 15%, the Cr^{6+}/Cr^{3+} ratio decreases from 1.30 to 1.21.

3.4 TPR Results

H_2-temperature programmed reduction (H_2-TPR) patterns of the Cr/SBA-15, 5Cr–Ce/SBA-15 and bulk Cr_2O_3 samples are depicted in Fig. 6. There is no obvious reduction peak of the SBA-15 support in the temperature range of 25–900 °C. For bulk Cr_2O_3, only one weak reduction peak appears in the profile at 440 °C, corresponding to the reduction of Cr^{6+} in the oxide [33]. For the Cr/SBA-15 catalyst with Cr content increasing from 2.5 to 10%, the reduction peak of Cr^{6+} to Cr^{3+} [31, 34, 35] species shifts to

Table 2 Surface concentration of the Cr elements

Catalyst	Cr (%)	Cr^{3+} BE (eV)	Cr^{6+} BE (eV)	Cr^{6+}/Cr^{3+}
5.0Cr/SBA-15	0.827	577.2	579.1	0.31
5.0Cr–5.0Ce/SBA-15	0.846	577.2	579.1	1.14
5.0Cr–7.5Ce/SBA-15	0.851	577.1	579.0	1.20
5.0Cr–10Ce/SBA-15	0.889	577.2	579.2	1.30
5.0Cr–15Ce/SBA-15	0.876	577.2	579.1	1.21

higher temperatures which are 467, 468, 471 and 473 °C, respectively, suggesting that the oxygen is more strongly bound in the dispersed chromium on the catalyst [36]. From Fig. 6c–f, it can be found that the H_2 consumption of Cr/SBA-15 sample increase until the Cr content reach 5%, whereas further increasing Cr content, the H_2 consumption decreases due to the formation of more crystal Cr_2O_3 phase, which is more difficult to reduce. Shi et al. [37] study results indicated the H_2 consumption of the peaks corresponds to the amount of Cr^{6+} species on Cr-based catalyst. In this paper, the TPR results suggests that 5Cr/SBA-15 has larger amount of the surface Cr^{6+} species than the other catalysts in all the Cr/SBA-15 catalyst. It is understandable that the percent of Cr^{6+} species increases with increasing Cr content under 5%. When the Cr content is above 5%, the percent of Cr^{6+} species decreases due to the formation of more crystal Cr_2O_3 phase.

The TPR profiles of 5.0Cr–Ce/SBA-15 show two overlapping reduction peaks at ca. 378 and 457 °C and a reduction peak at ca. 799 °C in Fig. 6g–j. The reduction peak appearing at ca. 457 °C corresponds to the reduction of Cr^{6+} to Cr^{3+} species. And the reduction peaks at ca. 378 and 799 °C are assigned to reduction of surface ceria oxide and the bulk CeO_2 in the 5Cr–Ce/SBA-15 catalyst, respectively [38]. Comparing the reduction peaks of 5Cr–Ce/SBA-15 sample with 10Ce/SBA-15 sample, it can be found that the reduction temperature of the ceria reduction decrease obviously. This indicates that there exists strong interaction between the Ce and Cr species and the interaction observably change the redox ability of Ce species. The H_2 consumption of the peak increases with the Ce loading from 5.0 to 10 wt.% and reach the maximum at 5.0Cr–10Ce/SBA-15 catalyst. That indicates the surface percent of Cr^{6+} species also reach maximum in the 5.0Cr–10Ce/SBA-15 catalyst. Further increasing Ce content to 15%, the H_2 consumption of Cr^{6+} reduction peak has a little decrease.

3.5 Catalytic Activity

Dehydrogenation of C_2H_6 over Cr/SBA-15 and 5Cr–Ce/SBA-15 catalysts with different Ce content in the presence or absence of CO_2 was investigated at 700 °C. The results are given in Table 3 The formation rate (TOF) of ethylene is calculated using the ethylene yield data the turnover frequency, defined in terms of ethylene moles formation per chromium atom per unit time. The SBA-15 support shows negligible C_2H_6 and CO_2 conversion. Over the catalysts, the major reaction product is C_2H_4, and the minor products are CH_4, CO, H_2 and H_2O in the presence of CO_2 atmosphere. After replacing CO_2 with Ar, the above products are also detected except for CO and H_2O products. In addition, the catalytic performances of the Cr/SBA-15 and 5Cr–Ce/SBA-15 catalysts in the present of CO_2 are obviously higher than that in the present of Ar, indicating the promoting effects of CO_2 for the ODH of ethane in the CO_2 atmosphere. For the Cr/SBA-15 catalysts, the maximum C_2H_6 conversion and C_2H_4 yield can be achieved on the 5Cr/SBA-15 catalyst. After Ce loading from 5 to 10%, the catalytic activity has obviously enhancement. The 55.0% ethane conversion and 52.8% C_2H_4 yield can be obtained on the 5Cr–10Ce/SBA-15 catalyst. Further increasing Ce content to 15%, the catalytic activity has some decrease. These results are agreement with the activation energy (Ep) values of the catalysts which are calculated from Arrhenius-type plots for the formation rate (TOF) of ethylene over 5.0Cr/SBA-15 and 5Cr–Ce/SBA-15 catalysts (Fig. 7). The TOF values of 5.0Cr–10Ce/SBA-15 are higher than the other catalysts in the range of measured temperatures, suggesting that active Cr sites in 5.0Cr–10Ce/SBA-15 is more effective to build ethylene molecules. The apparent activation energy for ethylene is in the range of 96.7–110.7 kJ/mol over the catalysts and this is in good agreement with previously published values

Table 3 Activity of the catalysts for the dehydrogenation of C_2H_6

Catalyst	In the presence of CO_2				Yield C_2H_4 (%)	In the presence of Ar			Yield C_2H_4 (%)	Ep (kJ/mol)
	Conv. (%)		Sel. (%)			Conv. (%)	Sel. (%)			
	C_2H_6	CO_2	C_2H_4	CH_4		C_2H_6	C_2H_4	CH_4		
SBA-15	2.7	0.04	93.5	6.5	2.53	2.4	93.0	7.0	2.23	–
2.5Cr/SBA-15	39.6	15.9	95.5	4.5	37.8	30.2	89.7	10.3	27.1	–
5.0Cr/SBA-15	46.3	16.6	94.7	5.3	43.8	34.1	91.4	8.6	31.2	110.7
7.5Cr/SBA-15	45.3	18.8	92.2	7.8	41.8	33.9	92.8	7.2	31.5	–
10Cr/SBA-15	44.2	18.9	92.0	8.0	40.7	31.2	90.9	9.1	28.4	–
5.0Cr–5Ce/SBA-15	48.4	17.9	96.4	4.6	46.7	35.8	87.6	12.4	31.4	108.5
5.0Cr–7.5Ce/SBA-15	50.0	20.9	96.0	4.0	48.0	37.9	88.2	11.8	33.4	103.8
5.0Cr–10Ce/SBA-15	55.0	21.9	96.0	4.0	52.8	40.8	83.1	16.9	33.9	96.7
5.0Cr–15Ce/SBA-15	52.2	21.2	95.5	4.5	49.9	40.1	82.4	17.6	33.0	99.1

Reaction conditions: GHSV = 3,600 mL/g h, $V_{CO_2 \text{ or } Ar}/V_{C_2H_6} = 3$, $T = 700$ °C

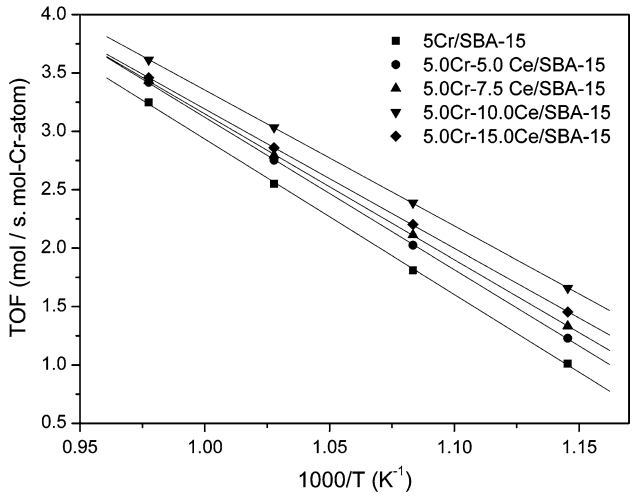

Fig. 7 Arrhenius plots for the formation rate of ethylene over 5Cr/SBA-15 and 5Cr–Ce/SBA-15 catalysts. Feed gas: GHSV = 9,600 mL g^{-1} h^{-1}, $V_{CO_2}/V_{C_2H_6} = 3$

from Mimura [39], who found 90 ± 3.0 kJ/mol energy barriers for dehydrogenation of ethane. The difference in the activation energy suggests that the both the number and nature of activity sites has changed after adding Ce species into the 5Cr/SBA-15 catalyst.

For the ODH of ethane over Cr-based catalyst, Chromium species with the high oxidation state were the key to higher catalytic activity during the ODH of ethane [31, 40]. In our case, the above TPR and XPS results also indicate that the appropriate addition of Ce species can increase reducibility of chromium and the ratio of Cr^{6+}/Cr^{3+} in the catalysts, which can well account for their different initial catalytic activities in the ODH of ethane. In addition, the higher catalytic activity of 5Cr–Ce/SBA-15 catalysts may also be caused by the present of Ce species, which was effective for the ODH of ethane with CO_2 and the redox Ce^{4+}/Ce^{3+} of CeO_2 can be used for the activation of CO_2 and produce active oxygen species for the reaction [41, 42].

The 5Cr–10Ce/SBA-15 with maximum Cr^{6+}/Cr^{3+} ratio displays the best catalytic activity for ODH of ethane with CO_2. This result indicates that the higher Cr^{6+}/Cr^{3+} ratio can increase the redox potential and has been reflected in the above the TPR profile. In addition, a redox mechanism is suggested for ODH of ethane in the presence of CO_2. Mimura et al. [39] used FTIR and XAFS to probe the active species and role of CO_2 for the ODH of ethane over Cr/H-ZSM-5 catalyst. They found that there existed a redox cycle involving Cr^{6+}/Cr^{3+} species in which a Cr^{6+} species was reduced to Cr^{3+} by ethane treatment, and CO_2 treatment led to reoxidation to Cr^{6+} species. On the basis of the current results, we believe that a high-oxidation-state Cr species is effective for the oxidative dehydrogenation. Indeed, the reduction of the Cr^{6+} to Cr^{3+} was demonstrated by the above TPR analysis. At the same time, the reduced Cr^{3+} species was also reoxygenated to Cr^{6+} species by CO_2 which will be proven by the following TPR, as a result, the high dehydrogenation activity Cr^{6+} species can be obtained by the Cr redox cycle during the ODH of ethane in the presence of CO_2. This means that CO_2 has a function of maintaining chromium oxide in higher oxidation states. That result again indicates the promoting effects of CO_2 for the ODH of ethane in the CO_2 atmosphere.

In addition, for the ODH of ethane with CO_2, considerable amounts of CO and H_2O are formed during the reaction, demonstrating the occurrence of a reaction between CO_2 and H_2 (water gas shift reaction). Removal of deposited carbon through the Boudouard reaction is another plausible cause. Water gas shift reaction can shift the dehydrogenation of ethane to product side, thus leading to the higher C_2H_6 conversion over these catalysts.

3.6 Deactivation and Regeneration

The catalytic performance over 5Cr/SBA-15 and 5Cr–10Ce/SBA-15 catalysts with reaction time and the regeneration by CO_2 were investigated, as shown in Fig. 8. Both the catalysts show high activity at the beginning of reaction. The activity gradually decreases during the reaction over the both catalysts. Especially, the conversions of C_2H_6 and CO_2 give a visible drop over the 5Cr/SBA-15 catalyst. For example, C_2H_6 conversion decreases from primal 46.4 to 23.6% over 5Cr/SBA-15 and 55.5 to 45.6% over 5Cr–10Ce/SBA-15, respectively, after reacting for 5 h. These results indicate a deactivation of both the catalysts, which could be associated with the reduction of active chromium (Cr^{6+}) species [31]. The disappearance of the active chromium (Cr^{6+}) oxide in the TPR pattern of the two catalysts after the dehydrogenation reaction of ethane (Fig. 9b) directly indicate the reduction of active chromium (Cr^{6+}) species, which can well account for the deactivation of two catalyst. On the other hand, the fall of the catalytic activity over 5Cr/SBA-15 is higher than that over 5Cr–10Ce/SBA-15 sample, suggesting that the addition of Ce also can increase the stability of 5Cr/SBA-15 due to their high thermal stability and better dispersion of the active metal.

After the reaction for 5 h, the gas flow of the mixture of C_2H_6 and CO_2 was replaced with a gas flow of CO_2 at 30 mL/min to treat with the catalysts for 12 h. It is noted the activity of 5Cr/SBA-15 and 5Cr–10Ce/SBA-15 catalysts was recovered insufficiently. Conversion of C_2H_6 over 5Cr/SBA-15 recovered from 23.6 to 30.9%, while that over the 5Cr–10Ce/SBA-15 recovered from 45.6 to 50.3%. At the same time, the TPR results also indicate that more active chromium (Cr^{6+}) species appear in the two catalysts (Fig. 9c).

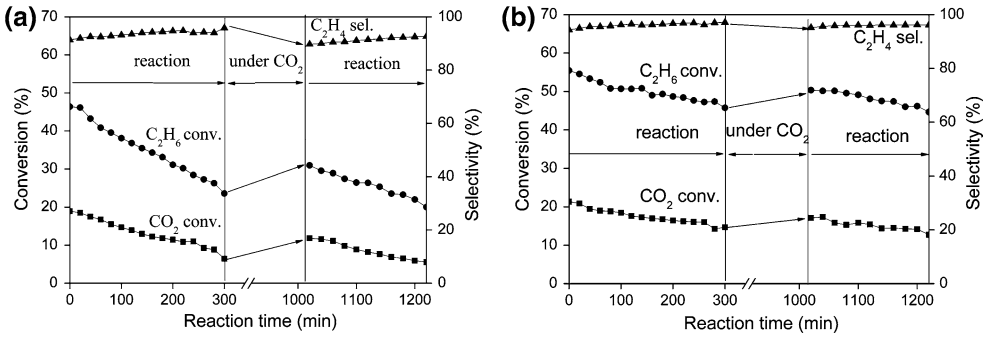

Fig. 8 Reactivity and regeneration with reaction time over 5Cr/SBA-15 (**a**) and 5Cr–10Ce/SBA-15 (**b**) catalysts. GHSV = 3,600 mL/g h, $V_{CO_2}/V_{C_2H_6} = 3$, $T = 700$ °C

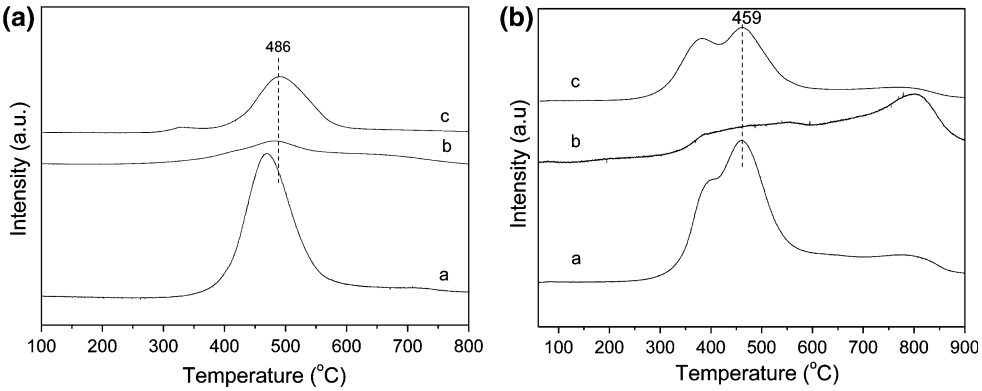

Fig. 9 TPR profiles of 5Cr/SBA-15 (**a**) and 5Cr–10Ce/SBA-15 (**b**) catalysts (a) before reaction, (b) after reaction (c) after regeneration by CO_2

The H_2-TPR profiles of the 5Cr/SBA-15 and 5Cr–10Ce/SBA-15 catalysts, including before and after reaction and after regeneration by CO_2 are shown in Fig. 9. Before reaction, the reaction peak at ca. 468 °C is attributed to the reduction of Cr^{6+} to Cr^{3+}. Similarly, the reaction peak at ca. 453 °C can also be attributed to reduction of Cr^{6+} to Cr^{3+} over the 5Cr–10Ce/SBA-15 catalyst. After reaction, the reduction peak became smaller, almost disappearing, over both catalysts, suggesting that most Cr^{6+} species were reduced to Cr^{3+} in the reaction. After treated by CO_2 at 700 °C for 12 h, the reduction peaks of Cr^{6+} species appear again. It is noteworthy that the maximum temperature (T_{max}) of reduction peak on the 5Cr/SBA-15 and 5Ce–10Ce/SBA-15 catalysts moves to high temperature region after regeneration, compared with that before reaction. This suggests the interaction between Cr species and SBA-15 or Ce/SBA-15 has changed in the reaction and regeneration treatment. For the fresh catalyst, the T_{max} of 5Cr–10Ce/SBA-15 is lower than that of 5Cr/SBA-15. This indicates that the Cr^{6+} species are prone to be reduced and served as the more active sites in 5Cr–10Ce/SBA-15 catalyst. This may be caused by the addition of Ce species which can supply mobile oxygen species, as a result, Cr^{6+} are easer reduced to serve as the active sites in the 5Cr–10Ce/SBA-15 catalyst.

4 Conclusion

Supported Cr–Ce/SBA-15 were prepared with well-ordered mesoporous structures and highly dispersed Cr and Ce species. The Cr–Ce/SBA-15 catalysts exhibit excellent catalytic activity at the ODH of ethane with CO_2. The 55.0% ethane conversion and 96.0% ethylene selectivity can be obtained over 5.0Cr–10Ce/SBA-15 catalyst at 700 °C. The high-angle XRD results suggest that the addition of Ce species obviously improve the Cr species dispersion in the Cr–Ce/SBA-15 catalysts. The low-angle XRD and N_2 sorption isotherms results indicate that the well-defined hexagonally ordered structure of the catalysts was not destroyed during the preparation process. TPR results indicate the Cr species in Cr/SBA-15 and 5.0Cr–Ce/SBA-15 catalysts existed with Cr^{6+} and Cr^{3+} species, and the Cr^{6+} species play an important role in the ODH of ethane with CO_2. The addition of Ce species to Cr/SBA-15 catalysts remarkably changes the redox properties and enhances the catalytic activity of Cr species in the 5.0Cr–Ce/SBA-15 catalysts. In addition, in the ODH of ethane with CO_2 reaction, the Cr^{6+} species as the active phase is reduced to Cr^{3+} as a less active species by the dehydrogenated process, simultaneously, the reduced Cr^{3+} species can be reoxidized to Cr^{6+} species by CO_2, and thus the

reduction–oxidation cycle between Cr^{6+} and Cr^{3+} species play an important role in the ODH of ethane with CO_2 reaction over the catalysts.

Acknowledgements Financial funds from the National Natural Science Foundation of China (Project Nos. 20473009) and the National Basic Research Program of China (Project No. 2005CB221405) are gratefully acknowledged.

References

1. Liu LC, Li HQ, Zhang Y (2006) Catal Today 115:235
2. Liu LC, Li HQ, Zhang Y (2007) Catal Commun 8:565
3. Wang SB, Murata K, Hayakawa T, Hamakawa S, Suzuki K (2000) Appl Catal A 196:1
4. Mimura N, Takahara I, Inaba M, Okamoto M, Murata K (2002) Catal Commun 3:257
5. Fujdala KL, Tilley TD (2003) J Catal 218:123
6. Cherian M, Rao MS, Deo G (2003) Catal Today 78:397
7. Nakagawa K, Okamura M, Ikenaga N, Suzuki T, Kobayashi T (1998) Chem Commun 1025
8. Takahara I, Saito M (1996) Chem Lett 973
9. Maity SK, Rana MS, Srinivas BN, Bej SK, Murali Dhar G, Prasada Rao TSR (2000) J Mol Catal A 153:121
10. Zhang X, Shi P (2003) J Mol Catal A 194:99
11. Rønning M, Huber F, Meland H, Venvik H, Chen D, Holmen A (2005) Catal Today 100:249
12. Kăspar J, Fornasiero P (2003) J Solid State Chem 171:19
13. Epling WS, Hoflund GB (1999) J Catal 182:5
14. Müller CA, Maciejewski M, Koeppel RA, Baiker A (1999) Catal Today 47:245
15. Zhao D, Feng J, Huo Q, Melosh N, Fredrickson GH, Chmelka BF, Stucky GD (1998) Science 279:548
16. Hartmann M, Vinu A (2002) Langmuir 18:8010
17. Burri DR, Jun K-W, Kim Y-H, Kim JM, Park S-E, Yoo JS (2002) Chem Lett 212
18. Zhang XZ, Yue YH, Gao Z (2002) Catal Lett 83:19
19. Liu YM, Cao Y, Yan SR, Dai WL, Fan KN (2003) Catal Lett 88:61
20. Lee SS, Park HI, Park BK, Byeon SH (2006) Mater Sci Eng B 135:20
21. Han P, Wang X, Qiu X, Ji X, Gao L (2007) J Mol Catal A 272:136
22. Burri DR, Choi K-M, Lee J-H, Han D-S, Park S-E (2007) Catal Commun 8:43
23. Berrichi ZE, Cherif L, Orsen O, Fraissard J, Tessonnier JP, Vanhaecke E, Louis B, Ledoux MJ, Pham-Huu C (2006) Appl Catal A 298:194
24. Vinu A, Sawant DP, Ariga K, Hartmann M, Halligudi SB (2005) Microporous Mesoporous Mater 80:195
25. Derossi S, Ferraris G, Fremiotti S, Garrone E, Ghiotti G, Campa MC, Indovina V (1994) J Catal 148:36
26. Kim DS, Wachs IE (1993) J Catal 142:166
27. Hakuli A, Kytökivi A, Krause AOI (2000) Appl Catal A 190:219
28. Liu B, Terano M (2001) J Mol Catal A 172:227
29. Hakuli A, Kytokivi A, Krause AOI, Suntola T (1996) J Catal 161:393
30. Mimura N, Takahara I, Okamato M, Murata K (2002) Catal Commun 3:257
31. Takehira K, Ohishi Y, Shishido T, Kawabata T, Takaki K, Zhang Q, Wang Y (2004) J Catal 224:404
32. Ge X, Zhu M, Shen J (2002) React Kinet Catal Lett 77:102
33. Cherian M, Yang WT, Jehng JM, Hirt AM, Deo G (2002) Appl Catal A 233:21
34. Gaspar AB, Brito JLF, Dieguez LC (2003) J Mol Catal A 203:251
35. Jiménez-López A, Rodrigues-Castellón E, Maireles-Torres P, Díaz L, Mérida-Robles J (2001) Appl Catal A 218:295
36. Pradier CM, Rodrigues F, Msrcus P, Landau MV, Kaliya ML, Gutman A, Herskowitz M (2000) Appl Catal B 27:73
37. Shi DX, Zhao Z, Xu CM, Duan AJ, Liu J, Dou T (2006) J Mol Catal A 245:106
38. A.Trovarelli , Zamar F, Llorca J, Leitenburg C, Dolcetti G, Kiss JT (1997) J Catal 169:490
39. Mimura N, Okamoto M, Yamashita H, Oyama ST, Murata K (2006) J Phys Chem B 110:21764
40. Mimura N, Takahara I, Inaba M, Okamato M, Murata K (2002) Catal Commun 3:257
41. Sharma S, Hilaire S, Vohs JM, Gorte RJ, Jen H-W (2000) J Catal 190:199
42. Valenzuela RX, Bueno G, Solbes A, Sapiňa F, Martínez E, Corberán VC (2001) Top Catal 15:181